First Clinicopathologic Evidence of a Non–PSMA-Related Uptake Mechanism for ^{68}Ga-PSMA-11 in Salivary Glands

Niels J. Rupp*[1], Christoph A. Umbricht*[2], Daniele A. Pizzuto[3], Daniela Lenggenhager[1], Antonia Töpfer[1], Julian Müller[3], Urs J. Muehlematter[3], Daniela A. Ferraro[3], Michael Messerli[3], Grégoire B. Morand[4], Gerhard F. Huber[5], Daniel Eberli[6], Roger Schibli[2], Cristina Müller†[2], and Irene A. Burger†[3]

[1]Department of Pathology and Molecular Pathology, University Hospital Zürich, University of Zürich, Switzerland; [2]Center for Radiopharmaceutical Sciences ETH-PSI-USZ, Paul Scherrer Institute, Villigen-PSI, Switzerland; [3]Department of Nuclear Medicine, University Hospital Zürich, University of Zürich, Switzerland; [4]Department of Otorhinolaryngology - Head and Neck Surgery, University Hospital Zürich, University of Zürich, Switzerland; [5]Department of Otorhinolaryngology - Head and Neck Surgery, Kantonsspital St. Gallen, Switzerland; and [6]Department of Urology, University Hospital Zürich, University of Zürich, Switzerland

The intense accumulation of prostate-specific membrane antigen (PSMA) radioligands in salivary glands is still not well understood. It is of concern for therapeutic applications of PSMA radioligands, because therapeutic radiation will damage these glands. A better understanding of the uptake mechanism is, therefore, crucial to find solutions to reduce toxicity. The aim of this study was to investigate whether the accumulation of PSMA-targeting radioligands in submandibular glands (SMGs) can be explained with PSMA expression levels using autoradiography (ARG) and immunohistochemistry (IHC). **Methods:** All patients gave written informed consent for further utility of the biologic material. The SMG of 9 patients, pancreatic tissue of 4 patients, and prostate cancer (PCA) lesions of 9 patients were analyzed. Tissue specimens were analyzed by means of PSMA-IHC (using an anti–PSMA-antibody and an immunoreactivity score system [IRS]) and ARG using ^{177}Lu-PSMA-617 (with quantification of the relative signal intensity compared with a PSMA-positive standard). The SUV_{max} in salivary glands, pancreas, and PCA tissues were quantified in 60 clinical ^{68}Ga-PSMA-11 PET scans for recurrent disease as well as the 9 primary tumors selected for ARG and IHC. **Results:** PCA tissue samples revealed a wide range of PSMA staining intensity on IHC (IRS = 70–300) as well as in ARG (1.3%–22% of standard). This variability on PCA tissue could also be observed in ^{68}Ga-PSMA-11 PET (SUV_{max}, 4.4–16) with a significant correlation between ARG and SUV_{max} ($P < 0.001$, $R^2 = 0.897$). On IHC, ARG, and ^{68}Ga-PSMA-11 PET, the pancreatic tissue was negative (IRS = 0, ARG = 0.1% ± 0.05%, SUV_{max} of 3.1 ± 1.1). The SMG tissue displayed only focal expression of PSMA limited to the intercalated ducts on IHC (IRS = 10–15) and a minimal signal on ARG (1.3% ± 0.9%). In contrast, all SMG showed a high ^{68}Ga-PSMA-11 accumulation on PET scans (SUV_{max} 23.5 ± 5.2). **Conclusion:** Our results indicate that the high accumulation of PSMA radioligands in salivary glands does not correspond to high PSMA expression levels determined using ARG and IHC. These findings provide evidence, that the significant accumulation of PSMA radioligands in SMG is not primarily a result of PSMA-mediated uptake.

Key Words: prostate cancer; prostate-specific membrane antigen; ^{177}Lu-PSMA-617; ^{68}Ga-PSMA-11; positron emission tomography; immuno-histochemistry; autoradiography

J Nucl Med 2019; 60:1270–1276
DOI: 10.2967/jnumed.118.222307

The prostate-specific membrane antigen (PSMA) is upregulated in prostate cancer (PCA), whereas only a few normal organs and tissue show physiologic expression (*1–3*). Currently, ^{68}Ga-PSMA-11 is widely used as a primary imaging tool for PCA restaging using PET at biochemical recurrence (*4,5*). It enables a high detection rate of small soft-tissue and bone lesions even at low prostate-specific antigen (PSA) values (*6*). The high and specific tumor uptake of ^{68}Ga-PSMA-11 prompted researchers to develop PSMA ligands with a DOTA-chelator (e.g., PSMA-617), for labeling with ^{177}Lu for therapeutic applications (*7,8*). Off-target uptake of PSMA radioligands was commonly detected in the kidneys, duodenum and small bowel, and lacrimal and major salivary glands (*9*). First dosimetry studies of ^{177}Lu-PSMA-617 revealed a significantly higher mean absorbed dose in salivary glands (1.4 Gy/GBq) than in kidneys (0.75 Gy/GBq) (*10*). This is in concordance with first results obtained after ^{177}Lu-PSMA-617 therapy, where no early nephrotoxicity, but some transient xerostomia in 8%–20% of the patients was observed (*7,11*). High salivary gland uptake is of particular concern when PSMA ligands are applied with α-particle emitters, such as ^{225}Ac, since this resulted in irreversible xerostomia and, hence, dose-limiting toxicity (*12,13*).

It was previously reported that PSMA is physiologically expressed on normal prostate epithelial cells, in the small intestine, renal tubular cells, and the salivary glands, however, at much lower levels than in PCA tissue (*13–15*). Other publications reported on immunohistochemical investigations, which showed no PSMA expression in salivary glands (*2,16,17*). These findings were in agreement with the fact that PSMA-specific radioimmunoconjugates, such as ^{111}In-J591 and ^{177}Lu-J591, did not accumulate in salivary glands (*18*).

A previous comment on the importance of salivary gland toxicity in PSMA-targeted radionuclide therapy stated the lack of sufficient data and understanding of the high uptake of PSMA ligands (*19*).

Received Nov. 13, 2018; revision accepted Jan. 13, 2019.
For correspondence or reprints contact: Irene A. Burger, Department of Nuclear Medicine, University Hospital Zürich, Rämistrasse 100, 8091 Zürich, Switzerland.
E-mail: Irene.burger@usz.ch
*Contributed equally to this work.
†Contributed equally to this work.
Published online Feb. 8, 2019.

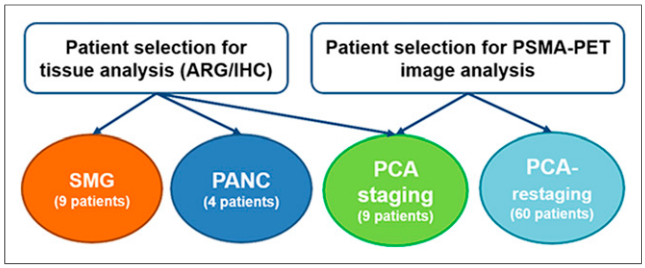

FIGURE 1. Overview of selected patients for tissue collection for ARG and IHC (SMG 01–09), pancreas (PANC 01–04), and primary PCA (PCA 01–09), as well as PSMA PET quantification, including the 9 patients with primary PCA (PCA 01–09) and 60 patients referred for restaging for the analysis of average uptake on salivary glands, pancreas, spleen, liver, and PCA metastasis.

Published mouse experiments do not reveal high accumulation of PSMA-targeting radioligands in salivary gland tissue (*20,21*). Therefore, such models are not suitable to investigate radiotherapy-related side effects to the salivary glands or methods to reduce salivary gland uptake of PSMA-targeting ligands.

The aim of this study was to compare the in vivo accumulation of ^{68}Ga-PSMA-11 in the PCA tissue, salivary glands, and pancreas of patients with the PSMA expression levels on PCA patient tissue, as well as to benign salivary gland and pancreatic tissue using immunohistochemistry (IHC) and in vitro autoradiography (ARG).

MATERIALS AND METHODS

Patients for IHC and ARG

Patients undergoing neck dissections including tumor-free submandibular glands (SMGs) were prospectively selected. Tissues of patients who underwent pancreas resection were included for the analysis of benign pancreatic tissue. All patients with prostatectomy for PCA and preoperative ^{68}Ga-PSMA-11 PET/MRI available were screened, and cases with tumor in the apex were selected, as fresh frozen tissue after standard prostatectomy was only available from the apex. For PET quantification in normal tissue, patients, referred to a ^{68}Ga-PSMA-11 PET for biochemical recurrence, were included. All patients gave written informed consent to further analysis of their data and biologic material within biobank protocols approved by the local ethics committee (BASEC no. 2016-00778, 2017-01319, KEK-StV-Nr: 40/08 and KEK-ZH-Nr. 06/08). The direct comparison to ^{68}Ga-PSMA-11 PET images was only possible for the PCA specimens. To determine the uptake of ^{68}Ga-PSMA-11 in PCA relative to the uptake in salivary glands and pancreas, an additional cohort of 60 patients who previously underwent ^{68}Ga-PSMA-11 PET for biochemical recurrence was included in a retrospective analysis (Fig. 1).

Tissue Preparation, PSMA IHC, and Evaluation

Fresh tissue of all types, obtained from the resection specimens immediately after surgery, was snap frozen. The remaining tissue was formalin-fixed, paraffin-embedded, and examined on 2-μm-thick hematoxylin & eosin (H&E)–stained sections. Both tissue types were compared microscopically to be representative. Immunohistochemical staining for PSMA (DAKO, M3620, clone 3E6, 1:25) was performed as described previously (*22*). PSMA expression was evaluated using a 3-tiered system (1+ weak, 2+ moderate, 3+ strong), and the area covered by staining was estimated in the following scale (1%, 2%, 5%, 10% followed by further 10% steps). Immunoreactivity score (IRS) was calculated as IRS = IHC expression score multiplied by the area covered (*23*). The area fraction covered by carcinoma and Gleason scores were determined by an experienced genitourinary pathologist after digitalization of the slides (Nanozoomer NDP digital slide scanner C9600-12) using the Hamamatsu NDP.view 2.6.8 Software.

TABLE 1
Patient Characteristics

Characteristic	*n*/mean	(%)/SD
SMG	9	
Age (y)	59	±13
Previous radiotherapy (yes)	3	33%
Pancreatic tissue	4	
Age (y)	66	±18
PCA tissue	9	
Age (y)	63	±5.4
PCA (+)	9	100%
PSMA PET scans	60	
Age (y)	67.3	±6.9
Activity (MBq)	136	±14.0
Weight (kg)	84.3	±10.8
No. of PCA metastasis	31	

In Vitro PSMA ARG

PSMA-617 (ABX GmbH) was labeled with no-carrier-added ^{177}Lu (ITG GmbH) under standard labeling conditions as previously reported (*20*). In vitro ARG was performed on frozen sections of patient tissue and mouse xenografts (highly PSMA-positive PC-3 PIP and PSMA-negative PC-3 flu tumors). In brief, buffer-treated sections were incubated with a solution of ^{177}Lu-PSMA-617 (1.5 MBq/mL in Tris-HCl buffer containing 1% bovine serum albumin) with or without blocking agent (200 μM 2-(phosphonomethyl)-pentandioic acid [2-PMPA; Sigma]) for 60 min at room temperature. Afterward, the sections were washed twice in cold Tris-HCl buffer (with 0.25% bovine serum albumin), twice in pure Tris-HCl buffer, and finally rinsed with cold distilled water. The air-dried sections were exposed to a phosphor imaging screen (Super Resolution; Perkin Elmer, USA)

TABLE 2
Comparison of the 9 Primary Prostate Tumors on Histology, ARG, and PSMA PET

Case	GS	H&E PCA-covered area (%)	PSMA IHC intensity	PSMA IHC % of tumor	PSMA IHC IRS	ARG (%)	PSMA SUV_{max}	PSMA SUV_{mean}
PCA 01	3 + 4	13	1	70	70	1.3	4.4	2.9
PCA 02	4 + 4	13	2	80	160	2.5	5.3	3.2
PCA 03	3 + 3	17	1	80	80	2.6	3.3	2.9
PCA 04	3 + 4	28	3	70	210	4.5	4.7	3.1
PCA 05	3 + 4	33	2	80	160	6.7	9.2	8.1
PCA 06	3 + 4	32	3	100	300	8.8	7.5	5.7
PCA 07	3 + 4	3	3	100	300	10.6	12.6	7.5
PCA 08	4 + 4	20	3	100	300	17.6	13.9	11.6
PCA 09	4 + 4	19	3	100	300	22.0	16	8.8

GS = Gleason score; covered area = carcinoma covered area of slide; IHC intensity = predominant IHC intensity; IHC % of tumor = percentage of carcinoma showing the predominant intensity; IHC IRS = predominant intensity × percentage of staining; ARG (%) = relative signal intensity on ARG; SUV_{max}/SUV_{mean} = in vivo accumulation of ^{68}Ga-PSMA-11.

that was developed using a radiometric phosphor imager (Cyclone Plus Storage Phosphor System; Perkin Elmer). The signal intensity on the autoradiographic images was quantified using the OptiQuant Acquisition software (version 5.0; Perkin Elmer). PC-3 PIP and PC-3 flu tumor xenograft sections were used as a positive or negative control, respectively. It is important to recognize that PSMA-transduced PC-3 (PC-3 PIP) tumors express PSMA reproducibly at levels much higher than pathophysiologic PSMA expression levels on human PCA (*24*). The percentage signal intensity relative to the PC-3 PIP section (set to 100%) was calculated. The images were arranged for visual display using Adobe Photoshop (version CS6; Adobe Systems, USA).

^{68}Ga-PSMA-11 PET/MRI

The 9 patients with primary PCA with corresponding tissue analysis underwent ^{68}Ga-PSMA-11 PET for staging of high-risk PCA between June 2016 and August 2017. For the second cohort of patients for PSMA PET image quantification, 60 consecutive patients referred for ^{68}Ga-PSMA-11 PET for biochemical recurrence were selected. All patients underwent a clinical routine whole-body PET/MRI 60 min after injection of ^{68}Ga-PSMA-11 using a hybrid scanner (SIGNA PET/MR; GE Healthcare) as reported previously (*25*). To quantify ^{68}Ga-PSMA-11 uptake, a standardized volume of interest (VOI) was positioned in the regular tissue of the parotid, submandibular, lacrimal, and sublingual glands, as well as pancreatic, hepatic, and splenic tissue to assess the maximum and mean SUV (SUV_{max} and SUV_{mean}, respectively). For patients with PSMA-positive local recurrence or metastasis, a VOI was placed over the most active lesion.

To quantify PSMA uptake on ^{68}Ga-PSMA-11 PET images in the 9 primary tumors, VOIs were placed into the apical quadrant positive for cancer on histopathology that was selected for further ARG and IHC analysis.

Statistical Analysis

Statistical analysis was performed with SPSS 25.0.0.0 software (IBM). Descriptive statistics was used to display patient data as median, SD, or number (percentage). The average activity or intensity on IHC, ARG, and PET imaging was correlated with the values obtained for SMG, pancreas, and PCA using Pearson correlation. A P value lower than 0.05 was considered to indicate statistical significance. Linear regression was used between the signal intensity on ARG and the uptake on PSMA PET to estimate the relation between PSMA expression and tracer uptake on ^{68}Ga-PSMA-11 PET images.

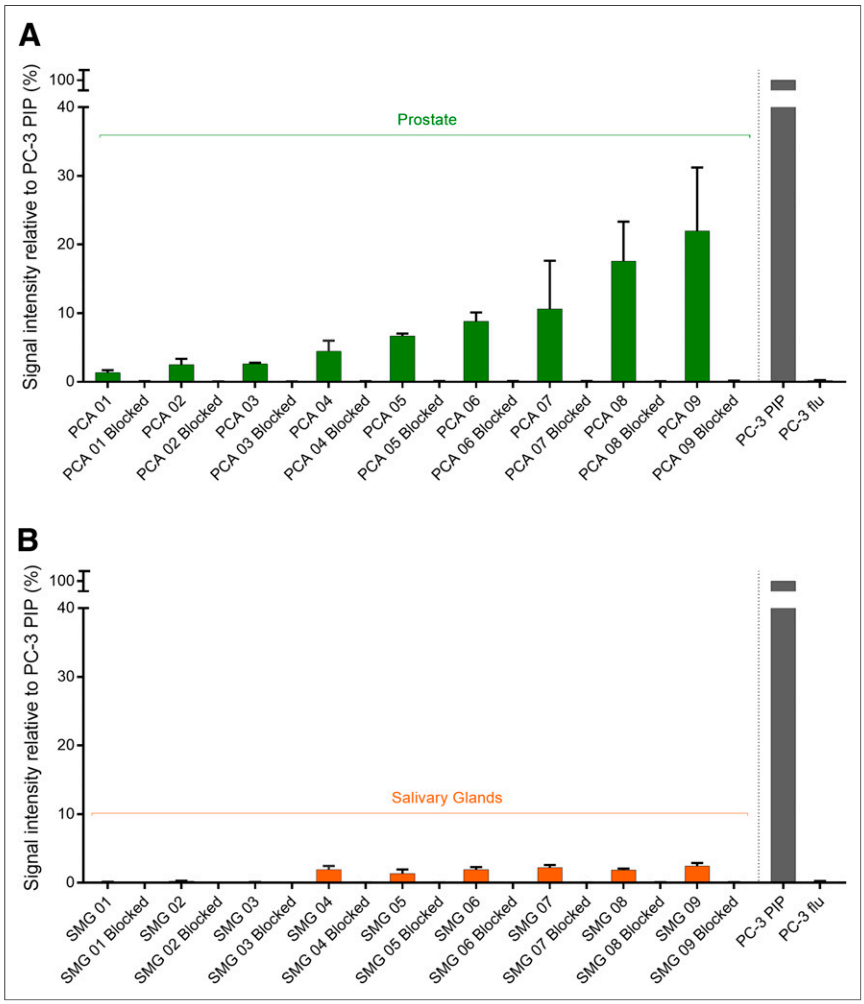

FIGURE 2. (A) ARG quantification of signal intensity of human primary PCA tissue relative to PC-3 PIP (high PSMA expression, set to 100%) and PC-3 flu (low PSMA expression) mouse tumor xenograft sections after application of ^{177}Lu-PSMA-617. Data shown for unblocked and 2-PMPA–blocked tissue sections. Heterogeneous pattern of signal intensity on ARG was observed, with mean of 8.5% ± 6.8% and range of 1.33%–21.98%, compared with PC-3 PIP tumor tissue. (B) Same ARG quantification for human salivary gland sections. SMG 01–03 with atrophy showed only minimal signal intensity (0.14% ± 0.10%) and SMG 04–09 with normal histology showed low signal intensity (1.94% ± 0.32%).

RESULTS

Patient samples for analysis of PSMA expression on SMG were isolated from 9 consecutive patients, for pancreatic tissue from 4 patients, and for PCA tissue from 9 patients with cancer in the apex. In 60 patients undergoing ^{68}Ga-PSMA-11 PET for restaging, the activity accumulation was determined in the lacrimal, parotid, submandibular, and sublingual gland, as well as in pancreatic, splenic, and hepatic tissue and in PCA lesions (Fig. 1; Table 1). In 31 patients, ^{68}Ga-PSMA-11–positive metastases were clearly localized. The mean uptake in the SMG was not different between patients with or without ^{68}Ga-PSMA-11–positive lesions with an SUV_{max} 23.5 ± 5.2 versus 23.3 ± 5.1 (P = 0.875), respectively.

PCA

Frozen tissue sections of the apex were analyzed in 9 patients with apical PCA confirmed on H&E staining. The area fraction covered by adenocarcinoma on the slides ranged from 3% to 33% and included Gleason scores from 3 + 3 to 4 + 4. The corresponding paraffin-embedded tissue stained with an anti-PSMA antibody indicated PSMA expression ranging from low (1+) to strong (3+), covering 70%–100% of the tumor tissue with IRS values between 70 and 300 (Table 2).

In analogy to the IRS score, the signal intensity on ARG images of PCA tissue

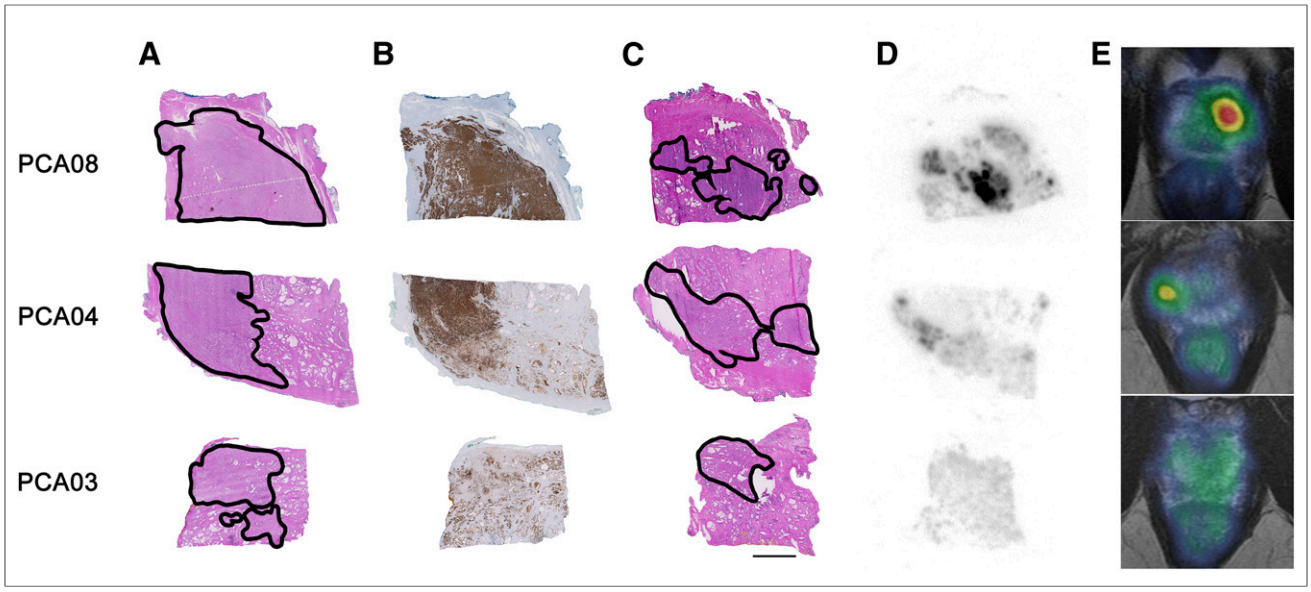

FIGURE 3. Comparison of 3 selected examples of prostate carcinomas (line by line) regarding hematoxylin & eosin (H&E) histology, PSMA IHC, in vitro ARG, and in vivo PET. Encircled carcinoma areas in formalin-fixed tissue (A), respective corresponding PSMA IHC (B), and selected encircled carcinoma areas in fresh frozen tissue (scale bar 5 mm) (C). D shows corresponding in vitro ARG with high (PCA08, GS 4 + 4), moderate (PCA04, GS 3 + 4), and low (PCA03, GS 3 + 3) normalized signal intensity on ARG, whereas E shows corresponding axial slice through apex of prostate on PSMA PET/MR. GS = Gleason score.

relative to PC-3 PIP tumor xenograft sections showed a heterogeneous pattern with a mean signal intensity of 8.5% ± 6.8% and a range between 1.3% and 22% (Fig. 2A). The pattern of signal intensity on frozen sections corresponded well with the tumor region on H&E histology.

Also, the in vivo ^{68}Ga-PSMA-11 accumulation determined on PET scans showed a heterogeneous SUV_{max} ranging from 4.4 to 16.0 in the areas of the investigated primary prostate adenocarcinoma corresponding to the signal seen on ARG (Table 2; Fig. 3).

Pancreatic Tissue

The healthy pancreatic tissue (PANC) was negative for PSMA on IHC in all 4 cases, even in the intercalated ducts (IRS 0; Table 3). The average signal intensity of the ARG performed on the pancreatic tissue was minimal in relation to PC-3 PIP tumor xenograft sections (0.1% ± 0.05%, Supplemental Fig. 1 [supplemental materials are available at http://jnm.snmjournals.org]), as was the case for the ^{68}Ga-PSMA-11 accumulation on ^{68}Ga-PSMA-11 PET scans that was low as well (SUV_{max} of 3.1 ± 1.1) (Table 4).

Salivary Glands

Three SMG were atrophic with signs of chronic inflammation, whereas 6 glands had a normal histology without inflammatory changes. IHC of PSMA expression showed distinct PSMA staining intensity (2 to 3+) that was limited in extent (5% of the tissue) and typically confined to the intercalated ducts of normal SMG, yielding an IRS of 10–15. Atrophic SMG showed a similar pattern, but markedly reduced staining intensity (1+), as well as decreased coverage (IRS of 2–5; Table 3; Figs. 4A and 4B). A minor, opaque and inconsistent staining of the mucinous glands was regarded as an unspecific artifact.

The average relative signal intensity on ARG images of SMG was 1.34% ± 0.89%. The 3 atrophic glands showed reduced signal intensity on ARG (0.14% ± 0.1%) compared with the 6 glands with normal histology (1.94% ± 0.32%) (Fig. 2B). Given that most PCA patients do not have atrophic salivary glands, further comparison was performed by considering only the average uptake of healthy SMG (Table 3).

In contrast to the low IRS on IHC and the minimal signal intensity on ARG, all SMG on ^{68}Ga-PSMA-11 PET scans revealed a strong accumulation of the tracer with a mean SUV_{max} of 23.5 ± 5.2 (range, 13.6–36.6) (Table 4; Fig. 5).

TABLE 3
Comparison of the 9 Salivary Gland and 4 Pancreatic Tissues

Case	Histology	PSMA IHC intensity	PSMA IHC % of tissue	PSMA IHC IRS	ARG (%)
SMG 01	Atrophic	1	5	5	0.1
SMG 02	Atrophic	1	2	2	0.2
SMG 03	Atrophic	1	2	2	0.1
SMG 04	Normal	2	5	10	1.9
SMG 05	Normal	3	5	15	1.4
SMG 06	Normal	3	5	15	1.9
SMG 07	Normal	2	5	10	2.2
SMG 08	Normal	2	5	10	1.8
SMG 09	Normal	2	5	10	2.4
PANC 01	Normal	0	0	0	0.0
PANC 02	Normal	0	0	0	0.1
PANC 03	Normal	0	0	0	0.2
PANC 04	Normal	0	0	0	0.1

PSMA IHC intensity = PSMA expression intensity; PSMA IHC % of tissue = percentage of tissue stained; PSMA IHC IRS = PSMA IHC intensity × PSMA IHC % of tissue; ARG (%) = relative signal intensity on ARG.

TABLE 4
Quantification of ^{68}Ga-PSMA-11 Accumulated in Different Tissues Based on PSMA PET

Tissue activity on PSMA PET (SUV_{max})	*n*	Minimum	Maximum	Mean	SD
Parotid	60	10.0	30.4	19.8	4.7
Submandibular	60	13.6	36.6	23.5	5.2
Lacrimal	60	6.0	25.8	13.8	4.2
Sublingual	60	3.6	31.0	10.7	4.6
Tonsils	60	3.0	12.6	7.8	2.1
Pancreas	60	0.4	5.4	3.1	1.1
Liver	60	4.1	16.3	8.2	2.6
Spleen	60	5.0	21.0	11.2	3.9
PCA tissue	31	2.7	48.7	15.9	11.8

Correlation Between IHC, ARG, and PET

The IRS evaluated by IHC and the ARG intensity showed a significant correlation ($R^2 = 0.642$, $P = 0.009$), visualizing the areas of PSMA-positive prostate adenocarcinoma. Furthermore, the ARG intensity correlated well with the accumulation of ^{68}Ga-PSMA-11 in the apical quadrant of the prostate as determined on PET images ($R^2 = 0.897$, $P < 0.001$) (Fig. 6).

In addition, SMG and pancreatic tissue displayed a significant correlation between the low IRS (mean SMG, 8.7 ± 4.9 and mean PANC, 0.0 ± 0.0) and the low ARG signal intensity (mean SMG, 1.3% ± 0.9% and mean PANC, 0.1% ± 0.1%, $R^2 = 0.739$, $P < 0.001$). In vivo accumulation of ^{68}Ga-PSMA-11 was strong in SMG, with a mean SUV_{max} of 23.5 ± 5.2 even surpassing the highest uptake detected in primary prostate adenocarcinoma (SUV_{max} 16.0 in PCA 09) (Fig. 6).

When a linear fit algorithm for ARG signal intensity and SUV_{max} was applied, over the 9 PCA cases, the following equation would result in (ARG %) = 1.46* (SUV_{max}) − 3.9. Assuming a similar perfusion between SMG tissue and PCA tissue, the same function should be applicable for ARG signal intensity and SUV_{max} on SMG. As a consequence, a mean ^{68}Ga-PSMA-11 uptake of SUV_{max} 23.5 determined on PET scans would correspond to an average signal intensity of 30% ((1.46 × 23.5) − 3.9) on ARG images. This would, however, be a 15-fold increased value as compared with the actual signal intensity of 1.9% determined for ARG images of normal SMG in our study.

DISCUSSION

The presented data support a mainly non–PSMA-related radioligand uptake in salivary glands, in contrast to a significant correlation of PSMA mediated radioligand uptake in primary PCA. IHC analysis showed a patchy and focal PSMA expression limited to the intercalated ducts in SMG, whereas serous acinar cells and striated ducts did not show PSMA expression.

On the SMG specimens with chronic sialadenitis and atrophy, the IHC staining pattern was similar but overall less intense. These data were confirmed by ARG analysis, which showed low signal intensity on SMG tissue. The pancreatic tissue, which has a histology similar to that of the SMG, did not show any expression of PSMA on IHC and ARG, respectively. The main structural difference between pancreatic tissue and SMG are the striated ducts (*26*). The substantial difference of PSMA radioligand uptake between these tissues may be attributed to the striated ducts. However, this

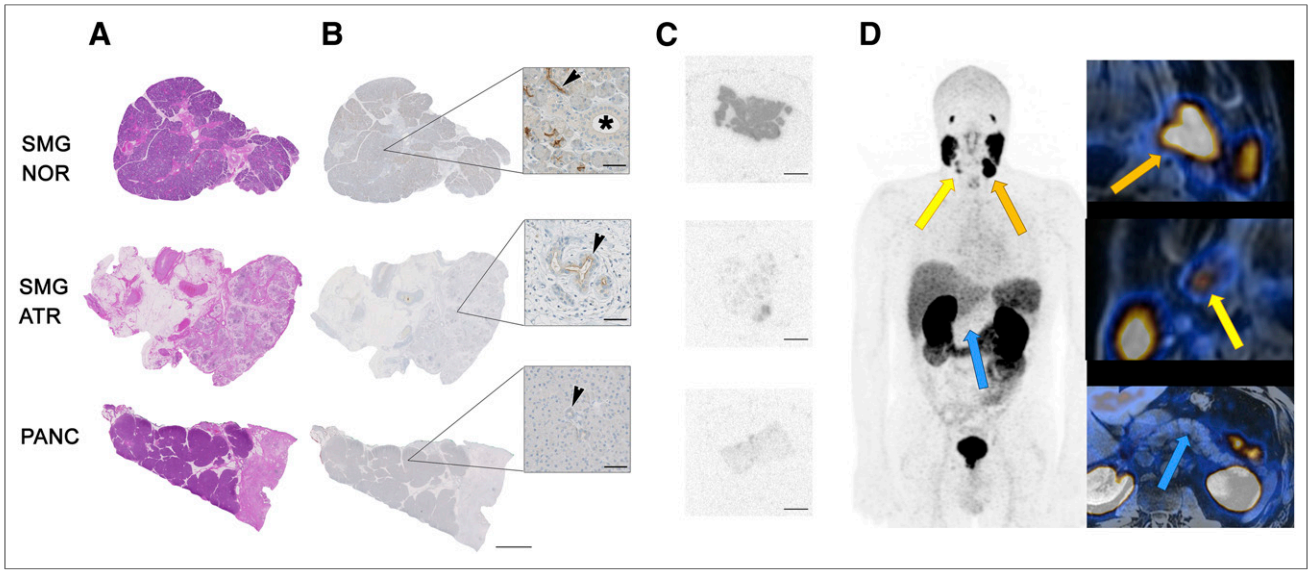

FIGURE 4. Comparison of normal and atrophic submandibular salivary gland tissue (SMG NOR and ATR), and pancreatic tissue (PANC) regarding hematoxylin & eosin (H&E) histology, PSMA IHC, and in vivo PET. (A) H&E histology of these 3 tissue types. (B) Moderate but focal PSMA expression in intercalated ducts (inset, arrow), whereas striated ducts (inset, asterisk) are PSMA-negative and intercalated ducts of atrophic salivary gland tissue show less expression. In pancreatic tissue, no PSMA expression is noted (inset, arrow shows negative intercalated duct). Scale bar 5 mm, and 100 μm (insets). (C) In vitro ARG with normalized signal intensity for normal and atrophic SMG besides normal pancreatic tissue. Scale bar 5 mm. (D) PSMA PET scan of patient showing high PSMA accumulation in left SMG (orange arrow, SUV_{max} 33), lower uptake in atrophic right SMG (yellow arrow, SUV_{max} 11), and only minimal uptake in pancreas (blue arrow, SUV_{max} 3) (magnification in insets).

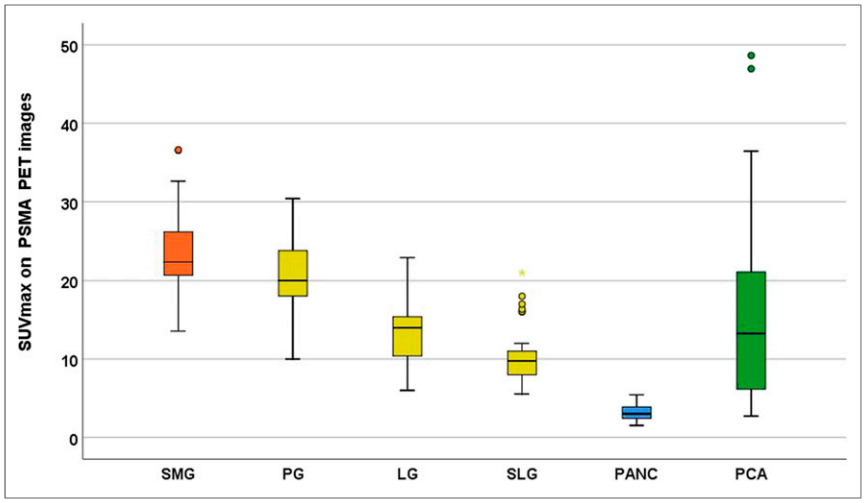

FIGURE 5. Box plots illustrating PSMA PET activity distribution for 60 consecutive patients imaged for PCA recurrence. High accumulation of ^{68}Ga-PSMA-11 60 min after injection can be measured in salivary glands of head and neck area, with a maximum in SMGs (orange), followed by parotid gland (PG), lacrimal gland (LG), and sublingual gland (SLG). Only minimal uptake was determined in pancreatic tissue (PANC, blue). Average ^{68}Ga-PSMA-11 uptake in SMGs was higher than uptake in PCA metastasis (PCA, green).

would be most likely PSMA-unrelated, as no PSMA expression is observed in the striated ducts.

The consistently high uptake of PSMA radioligands in all seromucous glands of the head and neck was also confirmed by Klein Nulent et al. with a retrospective analysis of 30 patients (*27*). Together with previous observations of minimal to patchy PSMA expression on IHC (*2,16,28*), this supports the hypothesis that the accumulation of small-molecule PSMA-targeting radioligands is largely nonspecific (*19*).

This could also explain why the injection of botulinum toxin into the salivary glands, which leads to a transient reduction in salivary gland function, reduces the PSMA radioligand accumulation up to 64% (*29*). Some clinicians suggested local cooling to reduce radioligand accumulation; however, the reduction of SUV_{max} by this measure was only 15%, so that further investigation is needed before consideration of clinical routine use (*30*). The approach of using inhibitors of PSMA (e.g., 2-PMPA) was found to be more successful in view of protecting the kidney from radiation damage (*31*), rather than the SMG, which was another finding supporting the hypothesis that the uptake of PSMA ligands in salivary glands is mostly PSMA-unrelated.

The sink effect in patients with high tumor burden is a phenomenon that led to a reduced radioligand accumulation in salivary glands (*32*); however, in the patients selected for this study referred for staging or early biochemical recurrence, the tumor burden was not high enough to affect the radioactivity uptake in the salivary glands.

A potential limitation of the present study may be that a direct comparison of the accumulation of PSMA radioligands in vivo, determined by PET examinations and in vitro using ARG of the same specimens for salivary gland and pancreatic tissue, is not possible. Given the consistent results for both pancreatic and normal SMG tissue regarding ARG and IHC, as well as the consistently high PSMA radioligand accumulation in salivary glands of the head and neck and low radioligand uptake in the pancreas, we believe that the indirect comparison as presented in this study is conclusive to confirm our hypothesis.

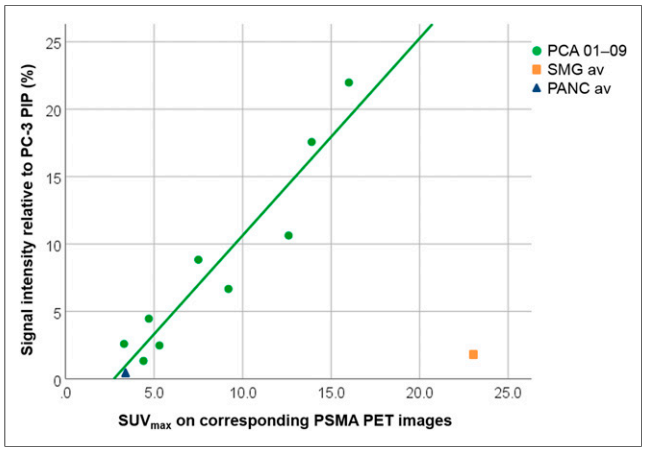

FIGURE 6. Scatterplot with linear regression fit for quantification of relative signal intensity on ARG images and corresponding quantification of in vivo uptake of ^{68}Ga-PSMA-11 on PET images (SUV_{max}) for PCA specimens (green, circle), with a linear regression fit ($R^2 = 0.897$, $P < 0.001$, y = 1.46*× −3.9). Average ARG signal intensity for salivary glands (SMG_{nor}, 1.94%) in relation to average SUV_{max} on 60 PSMA PET scans (SUV_{max} 23.5) is shown in orange (square) and ARG signal intensity for pancreases (PANC; 0.1%) in relation to average SUV_{max} on 60 PSMA PET scans (SUV_{max} 3.1) in blue (triangle).

CONCLUSION

Our data strongly suggest that accumulation of PSMA-targeting radioligands in salivary gland tissue is mainly nonspecific. Further studies will be necessary to investigate the exact mechanism of radioligand accumulation to develop new strategies to reduce radiotracer uptake in this dose-limiting tissues. This is in particular critical for radionuclide therapy using α-particle emitters with high linear energy transfer.

DISCLOSURE

Irene A. Burger has received research grants from GE Healthcare and Swiss Life and a speaker honorarium from GE Healthcare, Bayer Health Care, and Astellas Pharma AG. The Department of Nuclear Medicine holds an institutional research contract with GE Healthcare. No other potential conflict of interest relevant to this article was reported.

ACKNOWLEDGMENTS

We thank the Sick legat and the Iten-Kohaut foundation for their financial support. We acknowledge the technicians Marlena Hofbauer, Miguel Porto, Sofia Kaltsuni, and Sabrina Epp for their work on high quality PET/MR scans. We thank Susanne Dettwiler, Fabiola Prutek, and Christiane Mittmann for tissue processing and immunohistochemical stainings.

KEY POINTS

QUESTION: Is the high accumulation of PSMA-targeting radioligands in salivary glands due to a high PSMA expression?

PERTINENT FINDINGS: In this prospective study autoradiography (ARG, ^{117}Lu-PSMA-617) and immunohistochemistry (IHC, anti–PSMA-antibody) were performed on fresh frozen tissue from submandibular glands, pancreatic tissue, and prostate cancer. The correlation between SUV_{max} on ^{68}Ga-PSMA-11 PET and IHC PSMA expression and ARG signal intensity was very high (R^2 = 0.897) for prostate cancer whereas submandibular glands had only very limited PSMA expression on IHC and very low ARG signal intensity but a general high uptake on ^{68}Ga-PSMA-11 PET.

IMPLICATIONS FOR PATIENT CARE: We showed that the high accumulation of PSMA radioligands in salivary glands is not primarily a PSMA-mediated mechanism; therefore, other pathways and potential blocking methods need to be investigated to reduce the toxicity of PSMA radioligand therapy.

REFERENCES

1. Wright GL Jr, Haley C, Beckett ML, Schellhammer PF. Expression of prostate-specific membrane antigen in normal, benign, and malignant prostate tissues. *Urol Oncol.* 1995;1:18–28.
2. Silver DA, Pellicer I, Fair WR, Heston WD, Cordon-Cardo C. Prostate-specific membrane antigen expression in normal and malignant human tissues. *Clin Cancer Res.* 1997;3:81–85.
3. Perner S, Hofer MD, Kim R, et al. Prostate-specific membrane antigen expression as a predictor of prostate cancer progression. *Hum Pathol.* 2007;38:696–701.
4. Afshar-Oromieh A, Avtzi E, Giesel FL, et al. The diagnostic value of PET/CT imaging with the ^{68}Ga-labelled PSMA ligand HBED-CC in the diagnosis of recurrent prostate cancer. *Eur J Nucl Med Mol Imaging.* 2015;42:197–209.
5. Afshar-Oromieh A, Holland-Letz T, Giesel FL, et al. Diagnostic performance of ^{68}Ga-PSMA-11 (HBED-CC) PET/CT in patients with recurrent prostate cancer: evaluation in 1007 patients. *Eur J Nucl Med Mol Imaging.* 2017;44:1258–1268.
6. Kranzbühler B, Nagel H, Becker AS, et al. Clinical performance of ^{68}Ga-PSMA-11 PET/MRI for the detection of recurrent prostate cancer following radical prostatectomy. *Eur J Nucl Med Mol Imaging.* 2018;45:20–30.
7. Rahbar K, Ahmadzadehfar H, Kratochwil C, et al. German multicenter study investigating ^{177}Lu-PSMA-617 radioligand therapy in advanced prostate cancer patients. *J Nucl Med.* 2017;58:85–90.
8. Okamoto S, Thieme A, Allmann J, et al. Radiation dosimetry for ^{177}Lu-PSMA I&T in metastatic castration-resistant prostate cancer: absorbed dose in normal organs and tumor lesions. *J Nucl Med.* 2017;58:445–450.
9. Herrmann K, Bluemel C, Weineisen M, et al. Biodistribution and radiation dosimetry for a probe targeting prostate-specific membrane antigen for imaging and therapy. *J Nucl Med.* 2015;56:855–861.
10. Kratochwil C, Giesel FL, Stefanova M, et al. PSMA-targeted radionuclide therapy of metastatic castration-resistant prostate cancer with ^{177}Lu-Labeled PSMA-617. *J Nucl Med.* 2016;57:1170–1176.
11. Ahmadzadehfar H, Rahbar K, Kurpig S, et al. Early side effects and first results of radioligand therapy with ^{177}Lu-DKFZ-617 PSMA of castrate-resistant metastatic prostate cancer: a two-centre study. *EJNMMI Res.* 2015;5:114.
12. Kratochwil C, Bruchertseifer F, Giesel FL, et al. ^{225}Ac-PSMA-617 for PSMA-targeted alpha-radiation therapy of metastatic castration-resistant prostate cancer. *J Nucl Med.* 2016;57:1941–1944.
13. Kratochwil C, Bruchertseifer F, Rathke H, et al. Targeted alpha-therapy of metastatic castration-resistant prostate cancer with ^{225}Ac-PSMA-617: dosimetry estimate and empiric dose finding. *J Nucl Med.* 2017;58:1624–1631.
14. Israeli RS, Powell CT, Corr JG, Fair WR, Heston WD. Expression of the prostate-specific membrane antigen. *Cancer Res.* 1994;54:1807–1811.
15. Troyer JK, Beckett ML, Wright GL Jr. Detection and characterization of the prostate-specific membrane antigen (PSMA) in tissue extracts and body fluids. *Int J Cancer.* 1995;62:552–558.
16. Mhawech-Fauceglia P, Zhang S, Terracciano L, et al. Prostate-specific membrane antigen (PSMA) protein expression in normal and neoplastic tissues and its sensitivity and specificity in prostate adenocarcinoma: an immunohistochemical study using mutiple tumour tissue microarray technique. *Histopathology.* 2007;50:472–483.
17. Chang SS, Reuter VE, Heston WD, Bander NH, Grauer LS, Gaudin PB. Five different anti-prostate-specific membrane antigen (PSMA) antibodies confirm PSMA expression in tumor-associated neovasculature. *Cancer Res.* 1999;59:3192–3198.
18. Pandit-Taskar N, O'Donoghue JA, Morris MJ, et al. Antibody mass escalation study in patients with castration-resistant prostate cancer using ^{111}In-J591: lesion detectability and dosimetric projections for ^{90}Y radioimmunotherapy. *J Nucl Med.* 2008;49:1066–1074.
19. Taïeb D, Foletti JM, Bardies M, Rocchi P, Hicks RJ, Haberkorn U. PSMA-Targeted Radionuclide Therapy and Salivary Gland Toxicity: Why Does It Matter? *J Nucl Med.* 2018;59:747–748.
20. Umbricht CA, Benesova M, Schmid RM, et al. ^{44}Sc-PSMA-617 for radiotheragnostics in tandem with ^{177}Lu-PSMA-617-preclinical investigations in comparison with ^{68}Ga-PSMA-11 and ^{68}Ga-PSMA-617. *EJNMMI Res.* 2017;7:9.
21. Banerjee SR, Pullambhatla M, Foss CA, et al. ^{64}Cu-labeled inhibitors of prostate-specific membrane antigen for PET imaging of prostate cancer. *J Med Chem.* 2014;57:2657–2669.
22. Rupp NJ, Rechsteiner M, Freiberger SN, et al. New observations in tumor cell plasticity: mutational profiling in a case of metastatic melanoma with biphasic sarcomatoid transdifferentiation. *Virchows Arch.* 2018;473:517–521.
23. Remmele W, Stegner HE. Recommendation for uniform definition of an immunoreactive score (IRS) for immunohistochemical estrogen receptor detection (ER-ICA) in breast cancer tissue [in German]. *Pathologe.* 1987;8:138–140.
24. Umbricht CA, Benesova M, Schibli R, Müller C. preclinical development of novel PSMA-targeting radioligands: modulation of albumin-binding properties to improve prostate cancer therapy. *Mol Pharm.* 2018;15:2297–2306.
25. Sekine T, Barbosa FG, Sah BR, et al. PET/MR outperforms PET/CT in suspected occult tumors. *Clin Nucl Med.* 2017;42:e88–e95.
26. Orstavik TB, Brandtzaeg P, Nustad K, Pierce JV. Immunohistochemical localization of kallikrein in human pancreas and salivary glands. *J Histochem Cytochem.* 1980;28:557–562.
27. Klein Nulent TJW, Valstar MH, de Keizer B, et al. Physiologic distribution of PSMA-ligand in salivary glands and seromucous glands of the head and neck on PET/CT. *Oral Surg Oral Med Oral Pathol Oral Radiol.* 2018;125:478–486.
28. Gong MC, Chang SS, Sadelain M, Bander NH, Heston WD. Prostate-specific membrane antigen (PSMA)-specific monoclonal antibodies in the treatment of prostate and other cancers. *Cancer Metastasis Rev.* 1999;18:483–490.
29. Baum RP, Langbein T, Singh A, et al. Injection of botulinum toxin for preventing salivary gland toxicity after PSMA radioligand therapy: an empirical proof of a promising concept. *Nucl Med Mol Imaging.* 2018;52:80–81.
30. van Kalmthout LWM, Lam M, de Keizer B, et al. Impact of external cooling with icepacks on ^{68}Ga-PSMA uptake in salivary glands. *EJNMMI Res.* 2018;8:56.
31. Kratochwil C, Giesel FL, Leotta K, et al. PMPA for nephroprotection in PSMA-targeted radionuclide therapy of prostate cancer. *J Nucl Med.* 2015;56:293–298.
32. Gaertner FC, Halabi K, Ahmadzadehfar H, et al. Uptake of PSMA-ligands in normal tissues is dependent on tumor load in patients with prostate cancer. *Oncotarget.* 2017;8:55094–55103.